Electrochromic shift supports the membrane destabilization model of Tat-mediated transport and shows ion leakage during Sec transport

Anthony H. Asher[a] and Steven M. Theg[a,1]

[a]Plant Biology Department, University of California, Davis, CA 95616

Edited by Kenneth Keegstra, Michigan State University, East Lansing, MI, and approved February 8, 2021 (received for review August 27, 2020)

The mechanism and pore architecture of the Tat complex during transport of folded substrates remain a mystery, partly due to rapid dissociation after translocation. In contrast, the proteinaceous SecY pore is a persistent structure that needs only to undergo conformational shifts between "closed" and "opened" states when translocating unfolded substrate chains. Where the proteinaceous pore model describes the SecY pore well, the toroidal pore model better accounts for the high-energy barrier that must be overcome when transporting a folded substrate through the hydrophobic bilayer in Tat transport. Membrane conductance behavior can, in principle, be used to distinguish between toroidal and proteinaceous pores, as illustrated in the examination of many antimicrobial peptides as well as mitochondrial Bax and Bid. Here, we measure the electrochromic shift (ECS) decay as a proxy for conductance in isolated thylakoids, both during protein transport and with constitutively assembled translocons. We find that membranes with the constitutively assembled Tat complex and those undergoing Tat transport display conductance characteristics similar to those of resting membranes. Membranes undergoing Sec transport and those with the substrate-engaged SecY pore result in significantly more rapid electric field decay. The responsiveness of the ECS signal in membranes with active SecY recalls the steep relationship between applied voltage and conductance in a proteinaceous pore, while the nonaccelerated electric field decay with both Tat transport and the constitutive Tat complex under the same electric field is consistent with the behavior of a toroidal pore.

electrochromic shift | twin arginine translocon | Sec | protein translocation | toroidal pore

The twin arginine translocation pathway is uniquely able to transport fully folded substrates in an ATP-independent manner, relying instead on an electrochemical gradient (i.e., the proton motive force, or pmf) across the transporting membrane. It is crucial to the transport of substrates requiring various cofactors and hetero-oligomeric complexes in prokaryotes and of substrates vital to photosynthetic machinery in thylakoids (1). In plant mitochondria, the Rieske Fe/S protein required for the biogenesis of complex III is transported by the Tat pathway (2–6). It is implicated in both the virulence and antibiotic resistance of various infectious bacteria (7–12) and has been studied for its potential in biotechnology applications (13–15). The uniqueness of Tat functionality and its appearance across the kingdoms of life make it a valuable research target for crop modification, biotechnology, and pathogenesis. Unfortunately, much of the knowledge about its mechanism has been hard won, and the pore structure remains a mystery, likely due to the transient nature of the active complex.

The active Tat complex in thylakoids consists of three core subunits, Tha4, Hcf106, and cpTatC, which are homologous to the bacterial TatA, TatB, and TatC, respectively (1, 16). An N-terminal signal peptide with a twin-arginine motif inserts into the *cis*-side leaflet at the TatBC receptor complex (17–19). Subsequent oligomerization of TatA subunits (20–22) at the TatBC receptor complex results in rings of varying sizes (22, 23), but it is unclear whether these structures represent transport pores. Of particular note is the short TatA transmembrane helix (TMH). Composed of only 16 residues, the solid-state NMR solution suggests that the TMH must tilt and draw a portion of the *cis*-side amphipathic helix (APH) into the membrane in order to cross the bilayer (24), establishing a resting state of hydrophobic mismatch. During transport, a conformational shift increasing the angle between the TMH and APH results in exacerbated hydrophobic mismatch, as the APH is moved radially away from the center and the TMH is pulled up toward the *cis*-side in the active state (25, 26). For both native and foreign substrates, the Tat-targeted signal peptide and the pmf are sufficient to cause assembly of the active translocon and achieve transport (27–31). After the translocation event, the complex dissociates into TatA and TatBC components (1, 15, 16) with the exception of some residual TatA bound to the receptor complex in a nonactive state and a spectrum of smaller TatA oligomers (32).

Within the thylakoid membrane, it is useful to compare the Tat complex with the general secretory translocon (Sec) because they both function in the same membrane environment (1, 33). Sec translocation first requires recruitment of the substrate to the soluble SecA ATPase to form the substrate–SecA complex, which is then recruited to the SecY pore (1). In the inactive state,

Significance

Due to the transient nature of the active Tat complex, much of the knowledge available has been hard won. Electric-field-indicating absorbance transients allow investigation of transmembrane ion movement using native electric potential in thylakoids while circumventing challenges of reconstitution. Electrical behavior of transiently and/or constitutively assembled complexes suggests that Sec translocation occurs through a barrel-stave-type proteinaceous pore, while Tat translocation likely occurs through a toroidal pore. This would be the first instance of toroidal pores being exploited by a general protein translocation system. Our electrochemical analysis offers insight into how protein transport might be linked to light stimulation. Localized membrane destabilization presents a rational link between the proton motive force, membrane thinning, and Tat-mediated transport of substrates critical to photosynthesis.

Author contributions: A.H.A. and S.M.T. designed research; A.H.A. performed research; A.H.A. and S.M.T. analyzed data; and A.H.A. and S.M.T. wrote the paper.

The authors declare no competing interest.

This article is a PNAS Direct Submission.

See online for related content such as Commentaries.

[1]To whom correspondence may be addressed. Email: smtheg@ucdavis.edu.

Published March 15, 2021.

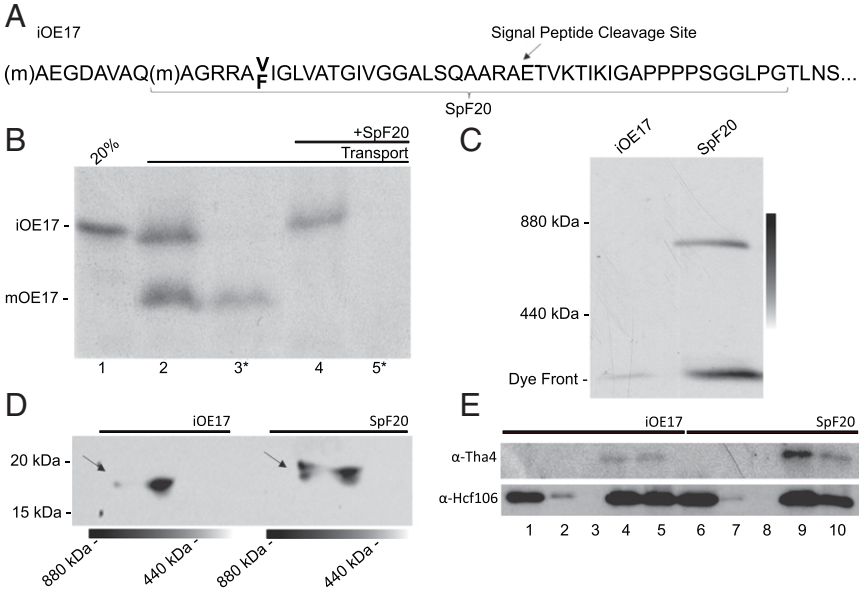

Fig. 1. SpF20 engagement of Tat components and constitutive assembly of the Tat complex. (*A*) The SpF20 substrate is an ∼5-kDa truncated form of the model substrate iOE17 that includes the Tat-targeted signal peptide and 20 amino acids of the mature region. (*B*) Transport of [^{3}H]-iOE17 is successful, as shown by the mature and thermolysin-resistant bands in lanes 2 and 3, respectively. Preincubation of membranes with SpF20 inhibited iOE17 transport (lanes 4 and 5). Asterisks denote thermolysin treatment. (*C*) Incubation of [^{3}H]-iOE17 and [^{3}H]-SpF20 with thylakoids under transport conditions yields an 800-kDa complex, indicating that the SpF20 substrate causes the assembly of a large complex that is similar in size to the previously described Tat complex (52). The gradient line represents the gel slab that was sampled in the second dimension. (*D*) Immunoblots of the BN-PAGE gel slabs run in the second dimension on SDS-PAGE were probed with α-Tha4 (TatA). The 800-kDa complex found in the BN-PAGE (arrows) after SpF20 treatment is enriched in Tha4. (*E*) Coimmunoprecipitation of the SpF20–TatABC complex by α-Hcf106 (TatB) beads is shown. Input (lanes 1 and 6), binding supernatant (lanes 2 and 7), wash volume (lanes 3 and 8), elution (lanes 4 and 9), and beads (lanes 5 and 10) from membranes with or without SpF20 are shown. Tha4 (TatA) signal in eluent lanes (lane 4 vs. lane 9) is significantly higher after SpF20 treatment, confirming constitutive complex assembly. Comparison of uneluted protein content (lanes 5 and 10) yields the same results.

the proteinaceous SecY pore prevents ion leakage through a combination of a *trans*-side plug domain and an internal array of hydrophobic residues (34). Following substrate–SecA docking, a conformational shift in SecY allows substrate movement through the open pore in an ATP-dependent process driven by SecA (35). In the mammalian homolog Sec61, leakage of NAD^+ ions is recorded during ribosome-bound nascent chain transport in a fluorescence quenching study, suggesting the pore can reach 4 to 6 nm in diameter (36). However, X-ray structures of substrate-fused SecA complexed with SecY (35), conductance studies in ribosome-bound substrates engaged with SecY (37), and SecY plug deletion mutants (38) in *Escherichia coli* have estimated the open SecY pore diameter to range from 7.3 to 8.8 Å, almost 10-fold lower. This small diameter likely contributes to the restriction of ion movement during Sec transport (39).

While the Sec machinery only transports unfolded substrates (40), the Tat pore accommodates substrates ranging from a single unfolded chain in an engineered system (13) to a folded substrate with an average diameter of 70 Å (41). This extended size range raises an interesting question about the pore architecture. In the Sec translocon, X-ray crystallography of the SecY channel in *Methanocaldococcus jannaschii* (42) and *Thermotoga maritima* (43) reveals that the SecY pore channel excludes lipids in both the resting state and when engaged with its SecA partner. Further structural work on the *E. coli* substrate-engaged SecA–SecY complex shows that the SecY channel excludes lipids during transport as well (35). No such structural information about the Tat pore exists, but functional data suggest that TatA plays an important role in the pore (20, 44, 45) and cryogenic electron microscopy structures of TatA oligomers reveal rings of an internal diameter ranging from 30 to 70 Å (23). During transport of the 17-kDa subunit of the oxygen-evolving complex (OE23), the Tat pathway exhibits very low ion leakage (46), estimated to be less than 1 pS. This is despite the exchange of 80,000 protons per substrate (47). Extensive mapping of subunit–subunit and subunit–substrate contacts has revealed no putative plug domain (20, 48–51) that could be compared to that in the SecY protein.

Pore architecture can be characterized by membrane conductance behavior. Conductance measured through proteinaceous pores representing the barrel-stave model has a very steep dependence on the voltage applied, whereas conductance in toroidal pores requires a larger voltage to be detected and increases more slowly in response to increasing voltage (52–54). Performing similar experiments on the Tat and Sec translocons would require functional reconstitution of both complexes into an in vitro setting. However, decay of the electrochromic shift (ECS) signal can be used as a measure of ion conductance (46). A transient absorption peak at ∼515 nm arising from carotenoid pigments in response to the native electric field generated by charge separation in the photosynthetic reaction centers (55) can be measured by delivering a single-saturating flash. The decay rate of such a signal is a direct measurement of how quickly the electric field is dissipated by ion movement across the membrane.

In the experiments reported herein, ECS signal decay rates revealing the conductance states of resting isolated membranes and those engaged in ongoing transport and in the presence of a constitutively assembled and/or substrate-engaged translocon are used to probe the pore architecture in the Tat and Sec complexes. Increased conductance across the thylakoid membrane is indicated by a more rapidly decaying ECS signal. We find that conductance in thylakoid membranes during Sec-mediated transport and substrate-engaged SecY is consistently higher than that during Tat-mediated transport and with the constitutively assembled Tat complex, respectively, despite the much

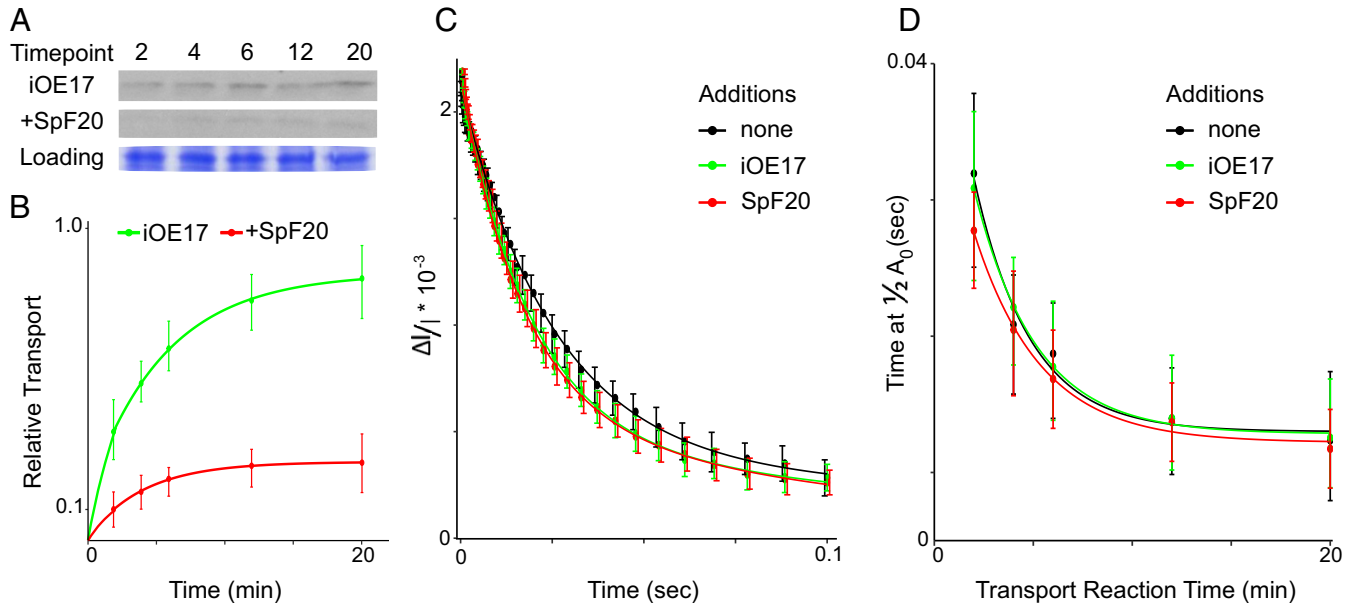

Fig. 2. Electric field decay during Tat-mediated transport and with the constitutively assembled complex. (*A*) Tat-mediated transport of radiolabeled iOE17, with or without preincubation with SpF20, was measured over 20 min in 1-mL cuvettes at 0.03 μg Chl μL^{-1} thylakoids under constant mixing. From the 1-mL transport reaction, 80 μL were harvested at each time point for SDS-PAGE. Representative films are shown with Coomassie-stained loading controls. (*B*) Quantitation of experiments in *A* where curves were normalized to the densest mature band in the single repetition for each of 12 repetitions and plotted with SD at each time point. (*C*) ECS decay profiles of isolated membranes, those with ongoing Tat-mediated transport, and those with constitutively assembled Tat complex at 6 min are plotted with 95% CIs. Results show strikingly little differences between the three states, indicating very little ion leakage despite the large average diameter of iOE17. (*D*) Times required to fall to half of the maximum ECS signal at 2-, 4-, 6-, 12-, and 20-min time points under 80 μE s^{-1} m^{-1} illumination in resting membranes, iOE17 transport, and the constitutively assembled Tat were averaged over 12 samples and plotted with CIs. No significant difference is seen between the three states, indicating no increase in ion leakage during transport or in the constitutively assembled state.

larger Tat pore required to transport a fully folded substrate. This points to a difference not only in mechanism but in pore architecture between the two. Conductance behavior of membranes undergoing Sec-mediated transport is consistent with that of a proteinaceous pore, while the resistance demonstrated by membranes undergoing Tat-mediated transport is more reminiscent of toroidal pores.

Results

Constitutive Assembly of the Active Tat Complex. The Tat complex appears to be transiently assembled in the presence of a Tat-targeted signal peptide and the pmf, then disassembled upon completion of the transport event (1, 15, 16). In thylakoids, the disassembly step can be inhibited when a severely truncated substrate is presented in vitro (20). We confirmed this using the truncated substrate SpF20 (Fig. 1 *A* and *B*). Thylakoids incubated with SpF20 under transport conditions and analyzed on blue native polyacrylamide gel electrophoresis (BN-PAGE) reveal that the predicted ~5-kDa substrate runs near 800 kDa (Fig. 1*C*), presumably with the Hcf106/cpTatC complex described earlier (56).

Peptide swapping experiments show that a Tat-targeted signal peptide and the pmf are sufficient for transport and thus are sufficient for the formation of the active-state translocon (27–31). To test for constitutive assembly, we next probed levels of Tha4, or TatA, in the Tat complex with and without SpF20 treatment. Gel excisions of the 440- to 880-kDa region from gradient BN-PAGE run in the second dimension reveal that the ~800-kDa Tat complex found after SpF20 treatment is enriched in TatA (Fig. 1*D*). For further confirmation, coimmunoprecipitation of the constitutively assembled Tat complex was performed with anti-Hcf106 (TatB) beads with and without SpF20 treatment. Thylakoids treated with SpF20 show enrichment of the TatA signal (Fig. 1*E*, lanes 4 and 9), demonstrating TatA recruitment to the Tat complex under SpF20 treatment. These results point to the constitutive assembly of the active Tat complex and an almost indefinite extension of the period under which electrical measurements can be made in isolated thylakoid membranes containing assembled Tat machinery.

ECS Decay during Ongoing Tat Transport and with the Constitutively Assembled Tat Complex. As seen repeatedly before, in vitro transport of Tat-targeted substrates followed an approximate exponential curve plateauing near 20 min (Fig. 2*A*). Pretreatment with SpF20 greatly reduced iOE17 transport over the entire lifetime of the reaction, bringing the final processed mature signal to 29% of the uninhibited counterpart (Fig. 2 *A* and *B*). In order to capture the ECS signal during active transport, the 6-min time point was chosen for comparison across resting membranes, membranes undergoing ongoing transport, and membranes with the constitutively assembled Tat complex.

The ECS signal during ongoing Tat-mediated transport demonstrated nearly the same decay profile as the resting isolated membranes. This is in keeping with previous work (46) indicating that the process is either somehow ion tight over the long term or that the active complex dissociates faster than ion movement through the pore can be detected. Binding of the SpF20 substrate results in the oligomerization of the active-state TatA in Fig. 1 and thus the constitutive assembly of the Tat complex (25). The ECS decay profile under SpF20 treatment exhibits no statistically significant difference from those of resting isolated membranes or those undergoing transport (Fig. 2*C*). Taken together, this implies that there is resistance to ion leakage at every stage of Tat translocation, unlike that which would be expected through an exclusively proteinaceous pore.

ECS signals were also measured at several time points over the 20-min transport reaction. The times required for the ECS signal to decay to one-half of its original amplitude at 2, 4, 6, 12, and

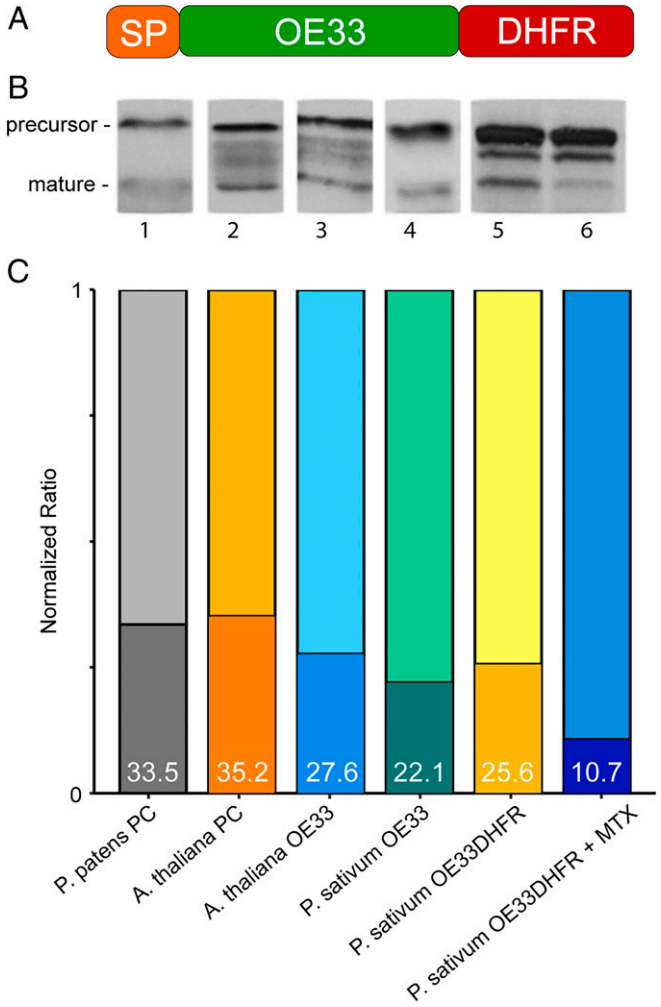

Fig. 3. Design of a DHFR-containing Sec substrate. (*A*) The Sec-targeted OE33 from *P. sativum* was fused with *E. coli* DHFR to create OE33DHFR. (*B*) Transport of OE33DHFR, with or without MTX, is compared to the transport of model substrates plastocyanin (lanes 1 and 2) and OE33 (lanes 3 and 4). Treatment with MTX severely inhibited OE33DHFR maturation (lane 6). Substrates were radiolabeled with [^{35}S]-methionine during in vitro translation and detected by autoradiography after transport. (*C*) Quantification of precursor and mature bands shown in *B* are summed and normalized to 1. The fraction of signal coming from the mature substrate is represented by shaded regions at the bottom of each bar and summarized by percentage in white text. Comparison within the group reveals that transport efficiency of the OE33DHFR substrate is neither anomalously high nor low but very close to the group median, suggesting that the DHFR fusion has a negligible effect on transport competence in our in vitro transport assay. *P. patens, Physcomitrella patens*; *A. thaliana*, *Arabidopsis thaliana*; *P. sativum*,*Pisum sativum*.

20 min were extracted and averaged across 12 replicates and plotted with 95% CIs (Fig. 2*D*). Ion leakage in transporting membranes and those with a constitutively assembled Tat complex displays virtually no difference from that of resting membranes.

Transport on the Sec Pathway. Extensive structural and mechanistic data for the homologous bacterial SecY have shown that the membrane-embedded pore is proteinaceous in nature yet still limits ion leakage. As such, it serves as a useful comparison when regarding the nature of the Tat pore, particularly because both the cpTat and cpSec systems function in parallel at the thylakoid membrane (1, 57).

In order to measure thylakoidal electrical behavior elicited by Sec-mediated transport and the substrate-engaged SecY pore, we probed this pathway using the Sec-targeted 33-kDa subunit of the oxygen-evolving complex fused to dihydrofolate reductase at the C terminus (OE33DHFR), represented by the cartoon in Fig. 3*A*. Transport of the OE33DHFR substrate was compared with that of several model Sec substrates (Fig. 3*B*) and found to be comparably robust. Methotrexate (MTX) is known to inhibit Sec transport by stabilizing the structure of the DHFR moiety (58, 59). Preincubation of OE33DHFR with MTX nearly abolishes formation of the mature signal (Fig. 3*B*). These results show that this fusion substrate is transported as well as other model substrates, while the DHFR moiety maintains its ability to bind MTX and can be expected to stall the substrate in midtransport, as previously demonstrated (58). Effectively, this allows us to generate three conductance states which can be compared to Tat transport: isolated resting membranes, those undergoing Sec transport, and those containing the substrate-engaged SecY pore.

ECS Decay during Ongoing Sec Transport and with the Substrate-Engaged Sec Complex. Similar to the transport shown in Fig. 2*A* for the Tat substrate iOE17, the appearance of mature OE33DHFR followed an exponential curve plateauing after 20 min (Fig. 4 *A* and *B*). Preincubation of the substrate with MTX significantly inhibited the formation of the final processed mature signal (Fig. 4 *A* and *B*). As in our Tat experiments, the 6-min time point was chosen to compare the three conductance states of the thylakoid membranes.

Fig. 4*C* shows that the ECS signal unexpectedly decayed significantly faster in membranes undergoing OE33DHFR transport and in those in which OE33DHFR is pretreated with MTX (Fig. 4*C*). This accelerated signal decay suggests that the SecY pore allows ion leakage across the thylakoid membrane during ongoing transport and when the substrate is stalled in midtransport. This behavior is markedly different from that found in ECS signals generated with Tat-engaged samples in Fig. 2*C*, where no increase in ion flow was observed.

Similar to Fig. 2*D*, ECS signals were again measured at several time points over the 20-min transport reaction. The decay time required to reach a half-maximum ECS signal, at each time point and in each membrane state, was then extracted and averaged over 12 replicates and plotted with 95% CIs (Fig. 4*D*). When compared to the resting membrane state (Fig. 4*D*, black curve), ECS decay rates were consistently faster during Sec-mediated transport (Fig. 4*D*, green curve) at each time point, although not significantly so in the earliest time points. The effect is slightly enhanced in the substrate-engaged, stalled-transport state (Fig. 4*D*, red curve).

Discussion

The Tat and Sec translocons work in parallel at the thylakoid membrane to transport proteins into the thylakoid lumen. The SecY channel is a stable and persistent proteinaceous pore that has evolved several mechanisms to prevent uncontrolled ion movement. In the homologous bacterial SecY, these mechanisms include a conserved network of six constricting hydrophobic residues in the pore channel itself (34) and, most notably, a plug domain on the *trans* side (38). In endoplasmic reticulum microsomes, there is additional evidence that the Hsp70 homolog BiP binds to the *trans* side of the channel to stem ion flow (60). While it is clear that TatA subunits can form a ring structure (23), no putative plug or conductance regulation domains have been identified. If TatA subunits were to form a proteinaceous channel resembling the barrel-stave model, it would be difficult to reconcile the tight control over ion movement during transport found in this work and previously (46) with conductance profiles of other barrel-stave pores formed by cell-penetrating

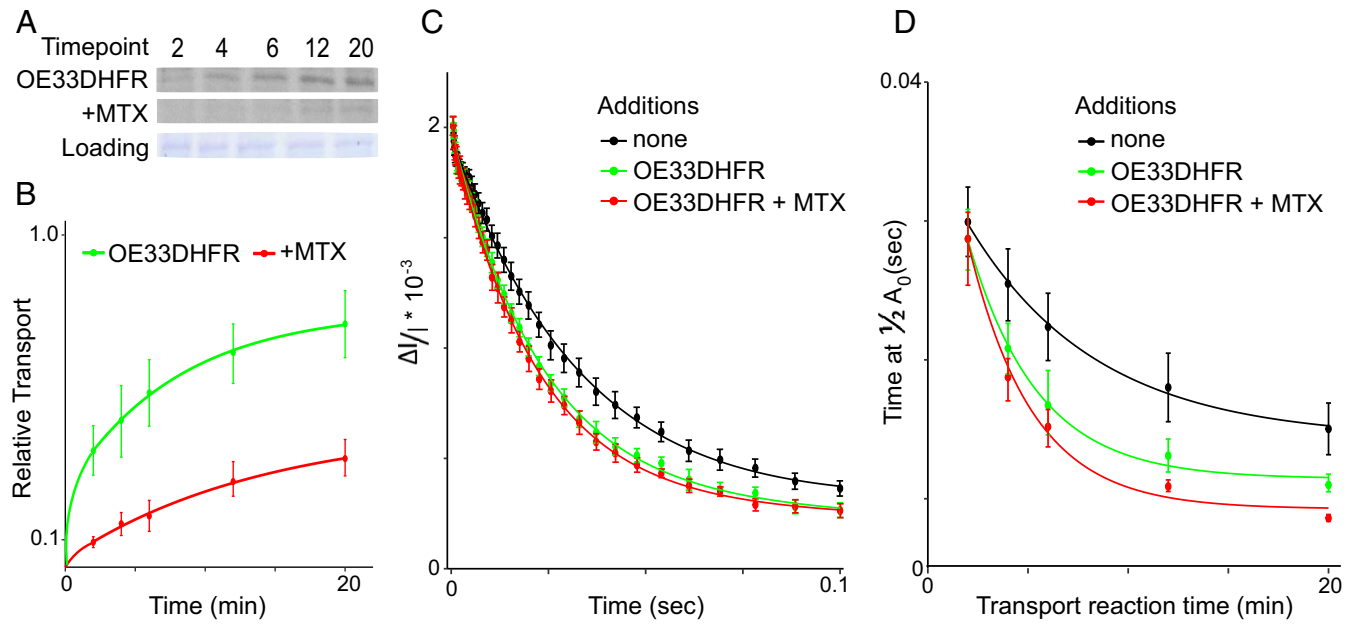

Fig. 4. Electric field decay during Sec-mediated transport and with the substrate-engaged SecY pore. (*A*) Sec-mediated transport of radiolabeled OE33DHFR, with or without preincubation with MTX, is carried out as in Fig. 2*A*. Representative films are shown with Coomassie-stained loading controls. (*B*) Mature band signals generated by transport of OE33DHFR and OE33DHFR + MTX are quantified and normalized as in Fig. 2*B*. (*C*) ECS decay profile of isolated membranes, those undergoing Sec-mediated transport, and those with the engaged SecY pore at 6 min are plotted with 95% CIs. Results show significant differences between the three, indicating leakage through the SecY pore when engaged with substrate. (*D*) Times required to fall to half of the maximum ECS signal at 2-, 4-, 6-, 12-, and 20-min time points under 80 μE s^{-1} m^{-1} illumination in resting membranes, during OE33DHFR transport, and during transport of the MTX-treated substrate are averaged over 12 samples and plotted with CIs. Transport of OE33DHFR and MTX-treated OE33DHFR caused significant acceleration of the decay of the ECS signal, indicating ion leakage in all cases where the proteinaceous SecY channel was targeted.

peptides (52, 54), mitochondrial channels (53), and cpSecY1 (Fig. 4 *C* and *D*).

ECS decay rates measured during Tat-mediated transport and with the constitutively assembled complex show essentially no difference from isolated resting membranes, following previous work showing that Tat-mediated transport is nearly ion tight (46). Successful transport of the OE17 substrate requires an estimated TatA oligomer comprising 26 copies (61), which, if arranged as a ring, would correspond to an internal channel diameter of 55 to 60 Å (23). This is nearly an order of magnitude larger than the SecY pore, whose open diameter ranges from 7.3 to 8.8 Å (35, 37, 38). The lack of change between the stalled Sec translocon and the actively transporting Sec complex was unexpected. In the stalled translocon, the pore should be held open, and ion movement was expected to increase. It is possible that the SecA bound to the translocon, or MTX-bound DHFR arrested within it, is able to physically block additional ion movement. We do not think this result affects our understanding of the mechanism of Sec transport. We do observe that conductance during Tat transport is significantly lower than that during Sec transport despite the larger internal diameter of the putative Tat pore.

In addition to discrepancies between the Tat pore size and conductance, any putative pore structure in the Tat complex must also accommodate polar residues on the surface of a fully folded substrate. While a highly conserved Glu residue in the TatA TMH provides a putative polar contact, this residue seems to be a part of a Pro-Glu motif that is more important as a contact point between Tat subunits (62). It is formally possible that there exists an undiscovered conformational intermediate exposing hydrophobic faces in the substrate only during transit, but surface hydrophobicity seems to block transport altogether (13). An exclusively proteinaceous TatA channel formed from the mostly hydrophobic TMH would likely create a prohibitive energy barrier to protein transport. When compared to the proteinaceous SecY pore, the Tat pore architecture must be radically different.

The membrane destabilization model (63) is an elegant alternative to a proteinaceous Tat pore, particularly in thylakoids (Fig. 5). Light stimulation causes global thinning of the thylakoid membrane (64, 65). Oligomerization of TatA subunits and a shift in conformation (25) focus and exacerbate thinning at the precise membrane patch where the bound substrate is located. Modeling data suggest that an indent in the bilayer surface bringing opposite leaflets closer together at a single point can result in the formation of a toroidal pore (66). The conformational shift in TatA results in increased hydrophobic mismatch by bringing the TMH closer to the *trans* side, creating a membrane deformation in an already thinned membrane. Under the electrochemical gradient across an energized membrane, this would lead to a controlled and localized bilayer breakdown precisely located where substrate is bound. As a toroidal pore forms, polar lipid head groups would likely be contacts between the pore wall and the polar surface residues of a folded transport substrate. This would also explain why small hydrophobic patches engineered into a substrate are able to abolish transport (13). Finally, membrane thinning upon energization provides a rational link between the pmf and Tat transport.

Typical voltage sweep experiments in reconstituted membranes measure the magnitude of current over a range of sustained voltages. In barrel-stave pores, the magnitude of the associated current at each voltage applied is higher than in membranes with toroidal pores (54). This indicates that charged species move more freely through barrel-stave pores, suggesting that either channel-type pores are more conductive or toroidal pores demonstrate resistance. This is a defining characteristic used to distinguish between the two pore archetypes (52–54). Our experiments are distinct from those above in that we

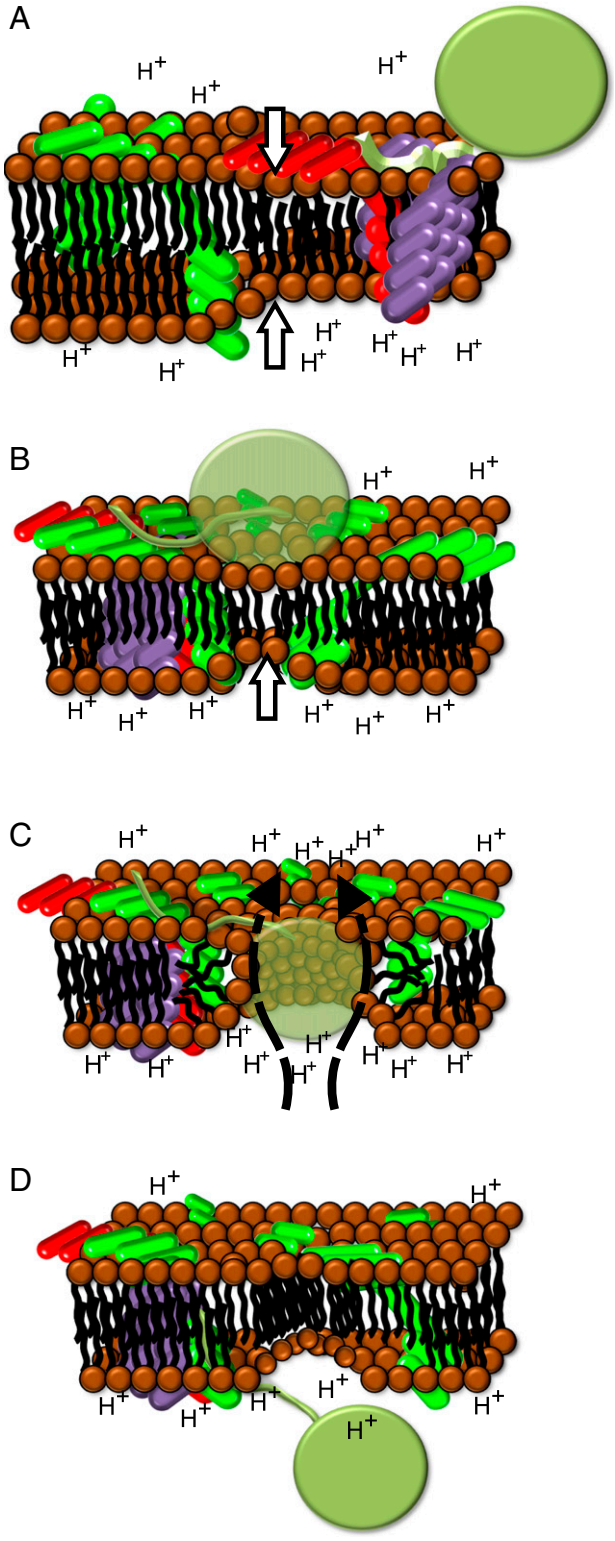

Fig. 5. A model of transport through the Tat complex. (*A*) Global thinning of the thylakoid membrane (white arrows) occurs as the pmf is generated. The signal peptide (light green) is bound, likely in a hairpin configuration (16) at the TatBC complex (red and purple). TatA (green) is dispersed throughout the thylakoid membrane. (*B*) Oligomerization of TatA into a ring and conformational shifts pulling the TMH toward the *cis* side increase hydrophobic mismatch and bring opposite leaflets closer together (white arrow). (*C*) Increased local TatA concentration in prethinned membrane creates targeted membrane destabilization, allowing the formation of a lipid-lined toroidal pore. As the folded substrate enters the pore, polar surface residues are accommodated by polar lipid heads lining the pore walls. A limited number of protons move from the lumen to stroma (dashed arrows). The resulting current is calculated to be below the detection limit of the ECS signal decay. (*D*) Following successful transport, the bilayer re-forms, and the Tat complex dissociates. The signal peptide is cleaved, releasing the substrate into the lumen.

monitor the change in membrane potential applied in microseconds and allowed to fall off. Since the rate of change of the voltage is proportional to the current flowing across the membrane, this experiment provides information analogous to the measurement of current during a voltage sweep. We have applied this to the collapse of the native electric field during Tat- and Sec-mediated transport. Under the electric field generated at the thylakoid membrane by a single saturating flash, ECS signal decay rates both during Tat-mediated transport and with the constitutively assembled Tat complex exhibit no difference from that of the resting isolated membranes (Fig. 2*C*). This is in direct contrast to the ECS signal decay in both Sec-mediated transport and the substrate-engaged SecY pore, where ECS decay is significantly faster than with resting membranes (Fig. 4*C*). Figs. 2*D* and 4*D* show that the electrical behavior distinguishing between barrel-stave-type channels and toroidal pores can also be seen when comparing Sec ECS signals with Tat ECS signals taken over the entire course of a transport reaction.

Our model of Tat-mediated protein translocation via transient toroidal pores is completely consistent with experiments showing that the mature domains of a transiting precursor make contact with all parts of cpTatA (50) and not, as would be expected in the proteinaceous pore model, just the portion that would constitute the putative pore. This model also offers insight into how protein transport is linked to the pmf in thylakoids. The light-induced global thinning of the membrane precedes the binding of the substrate signal peptide at the TatBC receptor complex (Fig. 5*A*). Global thinning of the thylakoid membrane is seen as a prerequisite for Tat-mediated transport and as such could signal a heretofore undescribed function of the pmf in addition to its role in ATP synthesis and ion homeostasis. Localized exacerbation of membrane thinning driven by TatA oligomerization (Fig. 5*B*) then results in bilayer breakdown with the formation of a transient toroidal pore (Fig. 5*C*) and, finally, the successful translocation of the substrate (Fig. 5*D*). Cross-linking experiments show the interaction of the substrate mature domain with the TatA APH and C-tail regions, indicating a *cis*-facing network that might prolong substrate presence at an actively assembling Tat complex (50). Such a network may be necessary in order for TatA recruitment to reach a critical mass and form a toroidal pore. This model thus expands the use of toroidal pores to their exploitation by a general, multisubstrate protein transport pathway.

Materials and Methods

Thylakoid Isolation. Chloroplasts isolated from *Pisum sativum* were osmotically lysed to yield thylakoids as in (67). Briefly, 9- to 10-d-old garden-variety pea leaves (Little Marvel) were homogenized in 1× grinding buffer (1xGB: 50 mM K-Hepes, pH 7.3, 0.33 M sorbitol, 1 mM $MgCl_2$, 1 mM $MnCl_2$, 2 mM ethylenediamine tetraacetic acid [EDTA], 0.1% bovine serum albumin). Chloroplasts were isolated in a continuous density Percoll gradient, osmotically lysed, then resuspended to 1 mg chlorophyll equivalents (Chl) mL^{-1} in 1× import buffer (1xIB: 50 mM K-Hepes, pH 8.0, 0.33 M sorbitol, 4 mM $MgCl_2$) for downstream applications.

Transport Assays. Transcription of the intermediate form of the 17-kDa oxygen-evolving complex subunit (iOE17) and the truncated iOE17, or SpF20, was performed in vitro using plasmids gifted by Ken Cline, University of Florida, Gainesville, FL (68) and Carole Dabney-Smith, Miami University, Miami, FL (20), respectively. The SpF20 substrate includes a truncated signal peptide and 20 amino acids of the mature region, along with the V20F

mutation that strengthens binding affinity (K_d ~1 nM) to the Tat machinery (61).

The precursor for the 33-kDa oxygen-evolving complex (OE33) complementary DNA (cDNA) from *Pisum sativum* (69) and dihydrofolate reductase (DHFR) cDNA from *Escherichia coli* (70) were fused by Gibson cloning, where the prOE33 was amplified using the primer 5′-CCCTCTAGAAATAATTTTGTT TAACTTTAAGAAGGAGATATACAT ATGGCAGCCTCACTTCAAGC-3′ and 5′-ACTGTAGTCACAGCTGAAGAGGATATCAT GCCGCCGCC AACACGCTCGCCTC-CAG -3′ and the DHFR in pET23 backbone was amplified using the primer 5′-CTGGAGGCGAGCGTGTT GGCGGCGGC ATCAGTCTGATTGCGGCGTTAGC-3′ and 5′-GCTTGAAGTGAGGCTGCCAT ATGTATATCTCCTTCTTAAAGTTAAAC-AAAATTATTTCTAGAGGG -3′. Transcription of *Ps*OE33-*Ec*DHFR (33DHFR) was performed in vitro with SP6 RNA polymerase (P1085) from Promega. Radiolabeled protein was translated with the Promega wheat germ lysate kit using either [H^3]-leucine or [S^{35}]-methionine.

Transport assays were composed of 10% vol/vol of wheat germ translation mixed in 1:1 ratio with 2xIB, 2.7 mM ATP, 0.33 μg Chl μL^{-1}, and 1xIB to make up the reaction volume. Transport reactions for Figs. 1 and 3 were performed in 60 μL. Transport reactions for ECS experiments were performed in a 1-mL cuvette with mixing. Each reaction was illuminated with 80 $\mu E\ s^{-1}\ m^{-2}$ for 20 min at room temperature and then analyzed on sodium dodecyl sulfate (SDS)-PAGE. Transport reactions in the Sec system were carried out identically to those in the Tat system, with the addition of overexpressed cpSecA1 (71) to 0.025 μg μL^{-1}.

BN-PAGE and Two-Dimensional Immunoblotting. Transport reactions were run as described above with iOE17 and SpF20. BN-PAGE was performed as described in (56). Briefly, each transport reaction was centrifuged at 1,000 × *g* and resuspended first in 10 μL of thylakoid solubilization buffer (0.5xIB, 20% glycerol, 0.5 M aminocaproic acid) and then mixed with 10 μL of thylakoid solubilization buffer containing 2% digitonin. Serva Blue G dye was added to each sample before running in a 1.5-mm 4 to 14% gradient gel. Ferritin oligomers were used for the molecular weight ladder.

For two-dimensional immunoblotting, the BN-PAGE gel was incubated at 37 °C in boiling buffer (65 mM Tris·HCl, pH 6.8, 20% SDS, 4% vol/vol β-mercaptoethanol in 300 mL ddH_2O) for 30 min. Gel slabs between 440 and 880 kDa were excised, rotated 90° counterclockwise, and run on a 15-mm 15% SDS gel for immunoblotting.

Coimmunoprecipitation. Isolation of assembled Tat complex after SpF20 treatment was performed as described in (20). Briefly, 20-min transport reactions with iOE17 or SpF20 were performed as described above in 60-μL reactions. Dithiobis(succinimidylpropionate) was added to a final concentration of 1 mM for 5 min and quenched with 10 mM Tris·HCl (pH 7.6). Thylakoid samples were solubilized with 1% SDS, 50 mM Tris·HCl (pH 7.6), 150 mM NaCl, and 0.5 mM EDTA for 10 min at 37 °C.

A dilution with 12.5 volumes of immunoprecipitation buffer (50 mM Tris·HCl, pH 7.6, 150 mM NaCl, 0.1 mM EDTA, 1% Triton X-100, and 0.5% deoxycholate) was followed by mixing with a 50-μL suspension of 50% magnetic α-Hcf106 beads. This was incubated at 4 °C for 3 h rotating end over end. Beads were washed three times with immunoprecipitation buffer before 15-s incubation with 20 μL of elution buffer (5% SDS, 0.1 M citric acid, pH 2.5). Eluted samples were then mixed immediately with 20 μL of 2.5 M Tris·HCl (pH 8). Cross-linked samples were reduced with β-mercaptoethanol at room temperature for 30 min before SDS-PAGE and immunoblotting.

Electrochromic Shift. In our ECS experiments, a single high-intensity saturating pulse of light was used to energize reaction centers throughout the entire sample. A low-intensity pulsed measuring beam was then used to monitor the 515-nm signal over time with microsecond resolution. Transport reactions were created on ice as above, then diluted fivefold into room-temperature-adjusted 1xIB in 1-mL cuvettes before making ECS measurements in a JTS 100 spectrophotometer (BioLogic). Single turnover saturating flashes were delivered from above using a Xenon arc flash lamp as in (46). Data were normalized to the point measured 0.1 ms after the flash.

Data Availability. All study data are included in the article.

ACKNOWLEDGMENTS. The authors acknowledge Dr. Carole Dabney-Smith, Dr. Kenneth Cline, and Dr. Kentaro Inoue for their generous sharing of resources and expertise and members of the S.M.T. laboratory for many discussions concerning these experiments. We gratefully acknowledge support from the Division of Chemical Sciences, Geosciences, and Biosciences, Office of Basic Energy Sciences of the US Department of Energy through Grant DE-SC0020304.

1. K. Cline, C. Dabney-Smith, Plastid protein import and sorting: Different paths to the same compartments. *Curr. Opin. Plant Biol.* **11**, 585–592 (2008).
2. E. G. Bogsch *et al*., An essential component of a novel bacterial protein export system with homologues in plastids and mitochondria. *J. Biol. Chem.* **273**, 18003–18006 (1998).
3. C. Carrie, S. Weißenberger, J. Soll, Plant mitochondria contain the protein translocase subunits TatB and TatC. *J. Cell Sci.* **129**, 3935–3947 (2016).
4. T. S. Weerakoon, Q. Ma, C. Dabney-Smith, Investigation of a mitochondrial twin arginine transport pathway in Arabidopsis thaliana. *FASEB J.* **30**, 1142.1 (2016).
5. B. Bennewitz, M. Sharma, F. Tannert, R. B. Klösgen, Dual targeting of TatA points to a chloroplast-like Tat pathway in plant mitochondria. *Biochim. Biophys. Acta Mol. Cell Res.* **1867**, 118816 (2020).
6. K. Schäfer *et al*., The plant mitochondrial TAT pathway is essential for complex III biogenesis. *Curr. Biol.* **30**, 840–853.e5 (2020).
7. L. Biswas *et al*., Role of the twin-arginine translocation pathway in Staphylococcus. *J. Bacteriol.* **191**, 5921–5929 (2009).
8. E. De Buck, E. Lammertyn, J. Anné, The importance of the twin-arginine translocation pathway for bacterial virulence. *Trends Microbiol.* **16**, 442–453 (2008).
9. U. A. Ochsner, A. Snyder, A. I. Vasil, M. L. Vasil, Effects of the twin-arginine translocase on secretion of virulence factors, stress response, and pathogenesis. *Proc. Natl. Acad. Sci. U.S.A.* **99**, 8312–8317 (2002).
10. N. Pradel, J. Delmas, L. F. Wu, C. L. Santini, R. Bonnet, Sec- and Tat-dependent translocation of β-lactamases across the Escherichia coli inner membrane. *Antimicrob. Agents Chemother.* **53**, 242–248 (2009).
11. N. Pradel *et al*., Contribution of the twin arginine translocation system to the virulence of enterohemorrhagic Escherichia coli O157:H7. *Infect. Immun.* **71**, 4908–4916 (2003).
12. K. Schaerlaekens *et al*., Twin-arginine translocation pathway in Streptomyces lividans. *J. Bacteriol.* **183**, 6727–6732 (2001).
13. S. Richter, U. Lindenstrauss, C. Lücke, R. Bayliss, T. Brüser, Functional Tat transport of unstructured, small, hydrophilic proteins. *J. Biol. Chem.* **282**, 33257–33264 (2007).
14. A. C. Fisher *et al*., Exploration of twin-arginine translocation for expression and purification of correctly folded proteins in Escherichia coli. *Microb. Biotechnol.* **1**, 403–415 (2008).
15. P. A. Lee, D. Tullman-Ercek, G. Georgiou, The bacterial twin-arginine translocation pathway. *Annu. Rev. Microbiol.* **60**, 373–395 (2006).
16. B. C. Berks, The twin-arginine protein translocation pathway. *Annu. Rev. Biochem.* **84**, 843–864 (2015).
17. M. Alami *et al*., Differential interactions between a twin-arginine signal peptide and its translocase in Escherichia coli. *Mol. Cell* **12**, 937–946 (2003).
18. K. Cline, H. Mori, Thylakoid DeltapH-dependent precursor proteins bind to a cpTatC-Hcf106 complex before Tha4-dependent transport. *J. Cell Biol.* **154**, 719–729 (2001).
19. S. Hamsanathan, T. S. Anthonymuthu, U. K. Bageshwar, S. M. Musser, A hinged signal peptide hairpin enables Tat-dependent protein translocation. *Biophys. J.* **113**, 2650–2668 (2017).
20. C. Aldridge, X. Ma, F. Gerard, K. Cline, Substrate-gated docking of pore subunit Tha4 in the TatC cavity initiates Tat translocase assembly. *J. Cell Biol.* **205**, 51–65 (2014).
21. C. Dabney-Smith, H. Mori, K. Cline, Oligomers of Tha4 organize at the thylakoid Tat translocase during protein transport. *J. Biol. Chem.* **281**, 5476–5483 (2006).
22. M. C. Leake *et al*., Variable stoichiometry of the TatA component of the twin-arginine protein transport system observed by in vivo single-molecule imaging. *Proc. Natl. Acad. Sci. U.S.A.* **105**, 15376–15381 (2008).
23. U. Gohlke *et al*., The TatA component of the twin-arginine protein transport system forms channel complexes of variable diameter. *Proc. Natl. Acad. Sci. U.S.A.* **102**, 10482–10486 (2005).
24. T. H. Walther, S. L. Grage, N. Roth, A. S. Ulrich, Membrane alignment of the pore-forming component TatA(d) of the twin-arginine translocase from Bacillus subtilis resolved by solid-state NMR spectroscopy. *J. Am. Chem. Soc.* **132**, 15945–15956 (2010).
25. C. Aldridge, A. Storm, K. Cline, C. Dabney-Smith, The chloroplast twin arginine transport (Tat) component, Tha4, undergoes conformational changes leading to Tat protein transport. *J. Biol. Chem.* **287**, 34752–34763 (2012).
26. F. Rodriguez *et al*., Structural model for the protein-translocating element of the twin-arginine transport system. *Proc. Natl. Acad. Sci. U.S.A.* **110**, E1092–E1101 (2013).
27. A. M. Chaddock *et al*., A new type of signal peptide: Central role of a twin-arginine motif in transfer signals for the delta pH-dependent thylakoidal protein translocase. *EMBO J.* **14**, 2715–2722 (1995).
28. S. A. Clark, S. M. Theg, A folded protein can be transported across the chloroplast envelope and thylakoid membranes. *Mol. Biol. Cell* **8**, 923–934 (1997).
29. M. P. DeLisa, D. Tullman, G. Georgiou, Folding quality control in the export of proteins by the bacterial twin-arginine translocation pathway. *Proc. Natl. Acad. Sci. U.S.A.* **100**, 6115–6120 (2003).
30. P. J. Hynds, D. Robinson, C. Robinson, The Sec-independent twin-arginine translocation system can transport both tightly folded and malfolded proteins across the thylakoid membrane. *J. Biol. Chem.* **273**, 34868–34874 (1998).
31. J. D. Thomas, R. A. Daniel, J. Errington, C. Robinson, Export of active green fluorescent protein to the periplasm by the twin-arginine translocase (Tat) pathway in Escherichia coli. *Mol. Microbiol.* **39**, 47–53 (2001).
32. J. Oates *et al*., The Escherichia coli twin-arginine translocation apparatus incorporates a distinct form of TatABC complex, spectrum of modular TatA complexes and minor TatAB complex. *J. Mol. Biol.* **346**, 295–305 (2005).

33. J. M. Celedon, K. Cline, Intra-plastid protein trafficking: How plant cells adapted prokaryotic mechanisms to the eukaryotic condition. *Biochim. Biophys. Acta* **1833**, 341–351 (2013).
34. B. Van den Berg *et al*., X-ray structure of a protein-conducting channel. *Nature* **427**, 36–44 (2004).
35. L. Li *et al*., Crystal structure of a substrate-engaged SecY protein-translocation channel. *Nature* **531**, 395–399 (2016).
36. B. D. Hamman, J.-C. Chen, E. E. Johnson, A. E. Johnson, The aqueous pore through the translocon has a diameter of 40-60 A during cotranslational protein translocation at the ER membrane. *Cell* **89**, 535–544 (1997).
37. I. Sachelaru *et al*., YidC and SecYEG form a heterotetrameric protein translocation channel. *Sci. Rep.* **7**, 101 (2017).
38. S. M. Saparov *et al*., Determining the conductance of the SecY protein translocation channel for small molecules. *Mol. Cell* **26**, 501–509 (2007).
39. E. Schiebel, W. Wickner, Preprotein translocation creates a halide anion permeability in the Escherichia coli plasma membrane. *J. Biol. Chem.* **267**, 7505–7510 (1992).
40. B. Ize, F. Gérard, L.-F. Wu, In vivo assessment of the Tat signal peptide specificity in Escherichia coli. *Arch. Microbiol.* **178**, 548–553 (2002).
41. T. Palmer, B. C. Berks, The twin-arginine translocation (Tat) protein export pathway. *Nat. Rev. Microbiol.* **10**, 483–496 (2012).
42. W. Li *et al*., The plug domain of the SecY protein stabilizes the closed state of the translocation channel and maintains a membrane seal. *Mol. Cell* **26**, 511–521 (2007).
43. J. Zimmer, Y. Nam, T. A. Rapoport, Structure of a complex of the ATPase SecA and the protein-translocation channel. *Nature* **455**, 936–943 (2008).
44. F. Alcock *et al*., Live cell imaging shows reversible assembly of the TatA component of the twin-arginine protein transport system. *Proc. Natl. Acad. Sci. U.S.A.* **110**, E3650–E3659 (2013).
45. P. Rose, J. Fröbel, P. L. Graumann, M. Müller, Substrate-dependent assembly of the Tat translocase as observed in live Escherichia coli cells. *PLoS One* **8**, e69488 (2013).
46. S. A. Teter, S. M. Theg, Energy-transducing thylakoid membranes remain highly impermeable to ions during protein translocation. *Proc. Natl. Acad. Sci. U.S.A.* **95**, 1590–1594 (1998).
47. N. N. Alder, S. M. Theg, Energetics of protein transport across biological membranes. A study of the thylakoid DeltapH-dependent/cpTat pathway. *Cell* **112**, 231–242 (2003).
48. N. P. Greene *et al*., Cysteine scanning mutagenesis and disulfide mapping studies of the TatA component of the bacterial twin arginine translocase. *J. Biol. Chem.* **282**, 23937–23945 (2007).
49. Q. Ma, K. Fite, C. P. New, C. Dabney-Smith, Thylakoid-integrated recombinant Hcf106 participates in the chloroplast twin arginine transport system. *Plant Direct* **2**, e00090 (2018).
50. D. Pal, K. Fite, C. Dabney-Smith, Direct interaction between a precursor mature domain and transport component Tha4 during twin arginine transport of chloroplasts. *Plant Physiol.* **161**, 990–1001 (2013).
51. S. Zoufaly *et al*., Mapping precursor-binding site on TatC subunit of twin arginine-specific protein translocase by site-specific photo cross-linking. *J. Biol. Chem.* **287**, 13430–13441 (2012).
52. M. Ashrafuzzaman, M. Duszyk, J. A. Tuszynski, Chemotherapy drugs thiocolchicoside and taxol permeabilize lipid bilayer membranes by forming ion pores. *J. Phys. Conf. Ser.* **329**, 012029 (2011).
53. A. J. García-Sáez *et al*., Peptides derived from apoptotic Bax and Bid reproduce the poration activity of the parent full-length proteins. *Biophys. J.* **88**, 3976–3990 (2005).
54. W. Hanke *et al*., Melittin and a chemically modified trichotoxin form alamethicin-type multi-state pores. *Biochim. Biophys. Acta* **727**, 108–114 (1983).
55. W. Junge, H. T. Witt, On the ion transport system of photosynthesis–Investigations on a molecular level. *Z. Naturforsch. B* **23**, 244–254 (1968).
56. F. Gérard, K. Cline, The thylakoid proton gradient promotes an advanced stage of signal peptide binding deep within the Tat pathway receptor complex. *J. Biol. Chem.* **282**, 5263–5272 (2007).
57. H. Mori, E. J. Summer, X. Ma, K. Cline, Component specificity for the thylakoidal Sec and Delta pH-dependent protein transport pathways. *J. Cell Biol.* **146**, 45–56 (1999).
58. T. Endo *et al*., Chloroplast protein import. Chloroplast envelopes and thylakoids have different abilities to unfold proteins. *Eur. J. Biochem.* **225**, 403–409 (1994).
59. M. Eilers, G. Schatz, Binding of a specific ligand inhibits import of a purified precursor protein into mitochondria. *Nature* **322**, 228–232 (1986).
60. B. D. Hamman, L. M. Hendershot, A. E. Johnson, BiP maintains the permeability barrier of the ER membrane by sealing the lumenal end of the translocon pore before and early in translocation. *Cell* **92**, 747–758 (1998).
61. J. M. Celedon, K. Cline, Stoichiometry for binding and transport by the twin arginine translocation system. *J. Cell Biol.* **197**, 523–534 (2012).
62. C. Dabney-Smith, H. Mori, K. Cline, Requirement of a Tha4-conserved transmembrane glutamate in thylakoid Tat translocase assembly revealed by biochemical complementation. *J. Biol. Chem.* **278**, 43027–43033 (2003).
63. T. Brüser, C. Sanders, An alternative model of the twin arginine translocation system. *Microbiol. Res.* **158**, 7–17 (2003).
64. S. Murakami, L. Packer, Light-induced changes in the conformation and configuration of the thylakoid membrane of Ulva and Porphyra chloroplasts in vivo. *Plant Physiol.* **45**, 289–299 (1970).
65. M. P. Johnson, A. P. R. Brain, A. V. Ruban, Changes in thylakoid membrane thickness associated with the reorganization of photosystem II light harvesting complexes during photoprotective energy dissipation. *Plant Signal. Behav.* **6**, 1386–1390 (2011).
66. S. J. Marrink, A. H. de Vries, D. P. Tieleman, Lipids on the move: Simulations of membrane pores, domains, stalks and curves. *Biochim. Biophys. Acta* **1788**, 149–168 (2009).
67. A. Asher, I. Ganesan, L. Klasek, S. M. Theg, Isolation of physiologically active thylakoids and their use in energy-dependent protein transport assays. *J. Vis. Exp.* **2018**, 58393 (2018).
68. K. Cline, W. F. Ettinger, S. M. Theg, Protein-specific energy requirements for protein transport across or into thylakoid membranes. Two lumenal proteins are transported in the absence of ATP. *J. Biol. Chem.* **267**, 2688–2696 (1992).
69. R. Wales, B. J. Newman, D. Pappin, J. C. Gray, The extrinsic 33 kDa polypeptide of the oxygen-evolving complex of photosystem II is a putative calcium-binding protein and is encoded by a multi-gene family in pea. *Plant Mol. Biol.* **12**, 439–451 (1989).
70. I. Ganesan, L. X. Shi, M. Labs, S. M. Theg, Evaluating the functional pore size of chloroplast toc and tic protein translocons: Import of folded proteins. *Plant Cell* **30**, 2161–2173 (2018).
71. J. K. Endow, R. Singhal, D. E. Fernandez, K. Inoue, Chaperone-assisted post-translational transport of plastidic type I signal peptidase 1. *J. Biol. Chem.* **290**, 28778–28791 (2015).